

Novel specular meteor radar systems using coherent MIMO techniques to study the mesosphere and lower thermosphere

Jorge Luis Chau¹, Juan Miguel Urco¹, Juha Pekka Vierinen², Ryan Andrew Volz³, Matthias Clahsen¹, Nico Pfeffer¹, and Jörg Trautner¹

¹Leibniz Institute of Atmospheric Physics at the University of Rostock, Germany

²UiT Arctic University of Norway, Norway

³MIT Haystack Observatory, USA

Correspondence to: J. L. Chau (chau@iap-kborn.de)

Abstract. Typical specular meteor radars (SMRs) use one transmitting antenna and at least a five-antenna interferometric configuration on reception to study the mesosphere and lower thermosphere (MLT) region. The interferometric configuration allows the measurement of the angle-of-arrival (AOA) of the detected meteor echoes, which in turn is needed to derive atmospheric parameters (e.g., mean winds, momentum fluxes, temperatures, and neutral densities). Recently, we have shown that coherent MIMO configurations in atmospheric radars, i.e., Multiple Input (transmitters) and Multiple Output (receivers), with proper diversity in transmission can be used to enhance interferometric atmospheric and ionospheric observations. In this study we present novel SMR systems using multiple transmitters in interferometric configuration, each of them employing orthogonal pseudo-random coded transmitted sequences. After proper decoding, the angle of departure (AOD) of the detected meteor echoes with respect to the transmitter site are obtained at each receiving antenna. We present successful bistatic implementations of (1) five transmitters and one receiver using coded continuous wave (CW) (MISO-CW), and (2) five transmitters and five receivers using coded CW (MIMO-CW). The latter system allows simultaneous independent observations of the specular meteor trails with respect to the transmitter (AOD) and with respect to the receiver (AOA). The quality of the obtained results is evaluated in terms of the resulting mean winds, the number of detections and the daily diffusion trail versus altitude behavior. We show that the proposed configurations are good alternatives to explore the MLT region. When combined with multi-static approaches, they can increase the number of meteor detections, thereby improving the quality of atmospheric estimates, and allowing the measurement of new atmospheric parameters (e.g., horizontal divergence, vorticity, etc.). The use of multiple collocated transmitters for interferometric AOD determination makes building a multistatic radar network logistically easier, as only one receiver per receiving site antenna is sufficient.

Copyright statement.

1 Introduction

In the last few decades specular meteor radars (SMR) have contributed significantly to the understanding of the mesosphere and lower thermosphere (MLT) region by providing continuous measurements of MLT parameters. Typical SMRs work in a monostatic configuration, i.e., the transmitting and receiving antennas are collocated. They provide routine measurements of altitude-resolved mean winds, temperatures, momentum fluxes, and neutral densities averaged over a few hundred kilometers in horizontal distance (e.g., Hocking et al., 2001; Holdsworth et al., 2004a; Hocking, 2005; Stober et al., 2014; Younger et al., 2015). Moreover, they are composed of a small number of antenna elements, are relatively easy to install, and are commercially available.

These systems are composed of a single transmitting antenna (or array) and a collocated multiple-receiver interferometric configuration. On transmission periodic pulses (coded and non-coded) are used. On reception, most of these radars use the so-called Jones configuration for the antenna layout (Jones et al., 1998) to determine the angle of arrival (AOA) of the meteor echoes. The main characteristics of the majority of such systems can be found in Hocking et al. (2001) and Holdsworth et al. (2004a).

To improve the number of detections and also to resolve winds inside the illuminated volume, Stober and Chau (2015) proposed the multi-static and multi-frequency approach, so called MMARIA (Multi-static, Multi-frequency Agile Investigations of the Atmosphere). The increased number of detections with respect to a monostatic system is due mainly to two factors: (1) new and independent detections of the same or different meteor trails are obtained in multi-static links, and (2) the effective Bragg wavelength is equal or larger than the monostatic Bragg wavelength therefore allowing the detection of larger radar-cross sections and higher altitudinal coverage (e.g., Stober and Chau, 2015).

The original MMARIA concept consisted of adding bistatic interferometric receive-only stations at distances between 60 to 200 km from existing transmitter sites. Vierinen et al. (2016) extended the concept by adding multiple coded continuous wave (CW) transmitter stations to be received by the existing network, each of them transmitting at the same frequency but with different orthogonal codes. Furthermore, Chau et al. (2017) implemented MMARIA using closely-located monostatic SMRs in northern Norway, transmitting at different frequencies. Preliminary wind field estimations in northern Germany using two pulsed transmitters with different frequencies, two coded CW transmitters, and five receiver stations have been recently presented by Stober et al. (2018).

As shown in Vierinen et al. (2016), the coded CW implementation presents many advantages with respect to traditional pulsed applications. Some of these advantages are: (1) for the same averaged power, the peak power is much less (e.g., 500 W instead of 10 kW for a pulsed transmitter with 5% duty cycle), (2) one could use the same frequency on different transmitting antennas with orthogonal codes, as is done in Global Position Systems, and (3) there are not range and Doppler ambiguities, which are present in pulsed systems.

Each of the MMARIA implementations mentioned above has proven to be challenging to deploy and operate, particularly for routine observations. For example, the Leibniz Institute of Atmospheric Physics (IAP), in conjunction with MIT Haystack Observatory, has implemented a coded-CW SMR network in northern Germany on campaign basis. One of the biggest challenges

during this project has been finding suitable locations for the transmitting stations in terms of security, societal perception of electromagnetic radiation hazards, legal issues, etc.

Urco et al. (2018) have shown that coherent multi-input (transmitters) multi-output (receivers) (MIMO) techniques can be useful for improving imaging and interferometric configurations in atmospheric and ionospheric radars. The techniques have been applied to studies of equatorial electrojet (EEJ) irregularities at the Jicamarca Radio Observatory (JRO), using three transmitting diversity schemes: time, polarization, and code. More recently Urco et al. (2019) has used MIMO with time diversity to study polar mesospheric summer echoes (PMSE) in northern Norway. MIMO techniques have been intensively investigated and used in the fields of communications, information theory, radar remote sensing, and over-the-horizon radars (e.g Telatar, 1999; Huang et al., 2011; Foschini and Gans, 1998; Frazer et al., 2007).

In this work we propose novel SMR systems that have emerged from the combination of our previous efforts and experiences. This includes the MMARIA concept (multi-static approach), the coded CW approach, statistical inverse-problems theory (e.g., compressed sensing), and the need to reduce some of the logistical issues experienced in previous efforts (e.g., finding multiple relatively large spaces for different receiving interferometers, finding allowable locations for single antenna coded CW transmitter stations, etc.). Our proposed systems make use of transmitting arrays in an interferometer-like configuration, with each antenna transmitting at the same frequency but with different codes, and accompanying receiver stations at distances between 20 to 200 km, with each station using one or more receiving antennas (multi-static). On reception, the signals from each transmitter station can be individually decoded and interferometrically combined to find the angle of departure (AOD) of the meteor echoes with respect to the transmitter station. This architecture limits most of the deployment complexity to a few interferometric transmitter stations while still providing the benefits of existing multi-static and coded CW approaches.

We start by describing the typical interferometer configurations of existing SMRs, i.e., using a single transmitter and multiple receivers. Then we present the details of the two systems that we have tested, both of them having the same multiple-transmitter geometry. The observations and results for each system are presented in Section 4 and compared with close-by observations of a standard SMR system. The advantages and challenges of the proposed systems are discussed in Section 5, including options for upgrading existing standard systems and, more importantly, ideas for future networks of multi-static SMRs.

2 Interferometry in standard specular meteor radars

Although SMRs have existed since War World II, they started to become more useful for atmospheric studies when they were able to measure the AOAs of the detected echoes by using suitable interferometer configurations. Given the large variability of signal strength of meteor echoes (more than 6 orders of magnitude), configurations able to resolve the AOA within the whole sky are needed, even when narrow transmitting antennas are used (e.g., Valentic et al., 1997).

Following the notation of Urco et al. (2018), the spatial coherence of a target located at (θ_R, ϕ_R) (elevation and azimuth) in the far-field with respect to the receiver interferometer, illuminated by transmitter p located at \mathbf{r}_p and received by a pair of receivers m and n located at \mathbf{r}_m and \mathbf{r}_n , respectively, is given by:

$$\rho(mnp)(\Delta\mathbf{r}_{mn}) \propto \exp(-j\mathbf{k}_R\Delta\mathbf{r}_{mn} + j\Delta\phi_{mn}), \quad (1)$$

where \mathbf{k}_R is the receiving wavenumber vector with $\mathbf{k}_R = 2(\pi/\lambda)[\cos\theta_R \cos\phi_R, \cos\theta_R \sin\phi_R, \sin\theta_R]$, λ is the radar wavelength, $\Delta\mathbf{r}_{mn} = \mathbf{r}_m - \mathbf{r}_n$ is the separation between receivers m and n , and $\Delta\phi_{mn}$ indicates the instrumental phase difference between receiver pair (m, n) . This expression corresponds to a coherent Single-input (transmitter) Multiple Output (receiver) (SIMO) configuration, depicted in Figure 1a. We are following this nomenclature to be consistent with a more general radar imaging problem when more than one target is present (e.g., Hysell and Chau, 2006).

For a deterministic target, an estimate of $\rho(mnp)$ given by $\hat{\rho}(mnp) \propto v_{mp}v_{np}^*$ is obtained from the correlation of the complex voltages at receivers m and n due to transmitter p , v_{mp} and v_{np} respectively. For stochastic targets, ensemble averages of this correlation are used (e.g. Urco et al., 2018, equation 2). At least two non-collinear pairs are needed to find the \mathbf{k}_r vectors (or AOAs).

Currently the most common configuration in standard SMRs is the so-called 5-antenna Jones interferometer (Jones et al., 1998). This configuration allows the possibility to resolve a short baseline for unambiguous determination and longer baselines for improving precision, in two orthogonal directions. The typical antenna separations are 2.0λ and 2.5λ . These pairs of antennas allow a simple algebraic solution to the AOA estimation by working with the phase information of equation 1 (e.g., Hocking et al., 2001; Holdsworth et al., 2004a). However, for improved estimation and for logistical purposes, other configurations have been used and suggested (e.g., Younger and Reid, 2017). In such cases, e.g., a pentagon configuration or antennas not necessarily located in a plane, the simple algebraic solutions are no longer applicable. On such configurations, Younger and Reid (2017) has proposed the used of pre-calculated phases, while Vaudrin et al. (2018) has proposed a complex fitting approach with the inclusion of uncertainty estimation of the resulting AOAs.

The phase difference between receivers m and n needs to be removed before the AOAs are estimated. Either they are measured using common feeding lines or echoes from targets with well known locations, or they are empirically estimated using the expected distribution of underdense specular meteor echoes (e.g., Valentic et al., 1997; Hocking et al., 2001; Holdsworth et al., 2004b; Lau et al., 2006; Chau et al., 2008; Chau and Clahsen, 2019).

25 3 Experiment configurations using multiple transmitters

A simple way to understand the benefits of coherent MIMO configurations is by presenting the interferometric expression of a MISO configuration, i.e., Multi-Input (transmitters) Single Output (receivers). The MISO configuration is depicted in Figure 1b. In this case the spatial coherence of a target located at (θ_t, ϕ_t) (elevation and azimuth) in the far-field with respect to the transmitter interferometer, illuminated by transmitters p and q located at \mathbf{r}_p and \mathbf{r}_q , respectively, and received by a single receiver m at \mathbf{r}_m , is given by:

$$\rho(mpq)(\Delta\mathbf{r}_{pq}) \propto \exp(-j\mathbf{k}_T \Delta\mathbf{r}_{pq} + j\Delta\phi_{pq}), \quad (2)$$

where \mathbf{k}_T is the transmitting wavenumber vector with $\mathbf{k}_T = 2(\pi/\lambda)[\cos\theta_T \cos\phi_T, \cos\theta_T \sin\phi_T, \sin\theta_T]$, $\Delta\mathbf{r}_{pq} = \mathbf{r}_p - \mathbf{r}_q$ is the separation between transmitters p and q , and $\Delta\phi_{pq}$ indicates the instrumental phase difference between transmitting pair (p, q) . Therefore the signal direction with respect to the transmitter \mathbf{k}_T (AOD), can be obtained from the cross-correlation of received signals at antenna m corresponding to transmitters p and q .

5 By combining the SIMO and MISO configurations, i.e., equations 1 and 2, respectively, the spatial coherence expression for a coherent MIMO configuration is given by:

$$\rho(mn pq)(\Delta \mathbf{r}_{mn}, \Delta \mathbf{r}_{pq}) \propto \exp(-j \mathbf{k}_R \Delta \mathbf{r}_{mn} - j \mathbf{k}_T \Delta \mathbf{r}_{pq} + j \Delta \phi_{mn} + j \Delta \phi_{pq}). \quad (3)$$

Following the notation of Stober and Chau (2015), the distance of the meteor echo to the transmitter and receiver are denoted by R_i and R_s , respectively.

10 A sketch of the MIMO configuration is given in Figure 1c. In the case of MISO and MIMO, the diversity on transmission is represented in Figure 1 using two different colors. Recall that such diversity, depending on the target and the system, could be in time, polarization or code. In the case of specular meteor echoes, polarization diversity is not an option since the different modes (ordinary or extraordinary) will suffer different amounts of group retardation (e.g, Elford, 2004). Based on the advantages described above, we find CW coding the most suitable diversity for our multistatic application. Below we discuss
 15 other possibilities using time diversity.

The above expressions are general for both monostatic and bistatic configurations. In the case of monostatic, the receiving (AOA) and transmitting (AOD) interferometric angles are the same with $\mathbf{k}_R = \mathbf{k}_T$, and the distances are also the same ($R_i = R_s$). Note that the expressions are given for far-field conditions with respect to each interferometer, i.e., the separation between interferometer antennas is much smaller than the distance to the meteor echo, $|\Delta \mathbf{r}_{mn}| \ll R_s$ and $|\Delta \mathbf{r}_{pq}| \ll R_i$ for the
 20 receiver and transmitter interferometers, respectively. In other words, MIMO provides the ability to “steer” the transmit beam on reception (in software), therefore providing the ability to maximize the transmit power incident on each meteor trail present in the field of view.

To implement our two multistatic multiple transmitter systems, we have used a transmitter array in Kühlungsborn and a receiver array in Neustrelitz (located ~ 123 km from Kühlungsborn). On transmission a 5-antenna 2.45λ equilateral pentagon
 25 configuration using a linear polarization was used. Different simultaneous orthogonal pseudo-random coded CW sequences were used on each transmitting antenna. The sequence was repeated every 10 ms. On reception, we used a 5-antenna Jones configuration using circularly-polarized antennas. Instead of the traditional 2.0λ and 2.5λ spacings, 1.0λ and 1.5λ spacings were used. Such a configuration has been successfully implemented at the Alta SMR in northern Norway. In the first implementation we used all five transmitting antennas and only one receiving antenna (MISO-CW). In the second one, we use all
 30 five receiving antennas (MIMO-CW).

The main experimental parameters of each system can be found in Table 1. For completeness, we are also including the parameters of the monostatic system located in Julisuruh that is used below as a reference. Note that all multiple transmitter experiments have been performed with customized transmitter and receiver hardware and software developed and integrated at IAP in collaboration with colleagues from MIT Haystack Observatory and the UiT Arctic University of Norway. On transmission, five CW Hilberling linear transmitters were used, and the wave forms generated on a PC and communicated to the transmitters by USRP-N200 units. On reception, multiple USRP-N200 units were also used. All the units were independently synchronized to the global reference clock using a Trimble Thunderbolt GPS disciplined oscillator (GPSDO). Currently none of these coded CW experiments could be implemented by existing commercially available SMR systems.

5 In the next section, we present the preliminary results of each system and some details of the decoding process. The specific details of the applied decoding processes in this work and those that are currently being improved will be given in a separate paper.

4 Results

The data quality of our proposed systems is compared qualitatively and quantitatively (when relevant) to observations made with a standard monostatic SMR located in Juliusruh in Northern Germany (13.37°E, 54.63°N). The main operational parameters of the Juliusruh radar are shown in Table 1. Following the nomenclature above, these observations are labeled SIMO-Pulsed.

Figure 2 shows selected measurements of basic parameters obtained on July 11-12, 2018 for the Juliusruh SMR: (a) time histogram, (b) 2D histogram of altitude versus inverse of meteor decay time (in linear scale), (c) altitude histogram, and (d) 2D histogram of latitude versus longitude (in linear scale). The total number of good counts are indicated in the time histogram plot in blue, while the number of detections with zenith angles less than 60° are indicated in black. In this particular campaign, close to 19,000 useful detections were obtained. In previous years for similar days, close to 24,000 meteors were observed using 30 kW peak power. In addition, zonal and meridional winds in one-hour and 2-km bins are shown in the second and third rows, respectively. These winds have been obtained with those detections within the white circle in Figure 2d (i.e., with zenith angles less than 60°). These observations are typical of the mid latitude mesosphere during summer months (e.g., Hoffmann et al., 2010).

The latitude vs longitude 2D histogram are overplotted over a geographic map. The location of the transmitter and receiver sites are indicated with white solid circles, in this case the same location. Note that Juliusruh is located 118 and 146 km from Kühlungsborn and Neustrelitz sites, respectively.

4.1 MISO-CW Results

In this section we present the results of the MISO-CW system that were obtained using the transmitter pentagon configuration described above and one circularly-polarized receiving antenna. The decoding process was done on signals from one receiving antenna using a compressed sensing approach on the complex raw voltages. Following a more common radar terminology, our procedure combines a matched filter estimator (MFE) and a Maximum Likelihood Estimator (MLE). The MLE is used to detect the strong echoes, whose signals are then removed from the complex voltages. After this initial identification and removal, an MFE is applied to go after the remaining medium to weak echoes. In both cases, the time and range location of the echoes is obtained. Finally a minimum least square error estimator is used to estimate the complex voltages of echoes at the pre-detected positions (time and range). In the case of a single transmitter, the MLE results could be equivalent to the results of an inverse filter, depending on the code selected. Our implementation is a modified version of a Generalized Orthogonal Matching Pursuit algorithm (Wang et al., 2012). Note that as a result of this processing, five different complex signals corresponding to each

transmitting antenna is obtained for each detected meteor. More details and discussion of the techniques implemented here and those being developed will be given in a separate paper.

5 Figure 3 shows an example of range time intensity (RTI) from a MISO-CW system obtained on July 12 at 0509 UT. The decoded signals of five synthetic receivers corresponding to all five transmitters and just one physical receiving antenna have been incoherently integrated. Note that more than 30 specular meteor echoes are observed with a naked eye, along with echoes from an airplane.

An identification process based on the works of Hocking et al. (2001) and Holdsworth et al. (2004a) was applied on the
10 complex voltages of the detected events. In this process we determine, among other parameters, total range detection, Doppler frequency, AODs, correlation time, detection time, etc., of each meteor echo. Namely, the AOD is obtained from the cross-correlation of the complex voltages corresponding to different transmitting antennas, while the Doppler and correlation times are obtained from the averaged autocorrelation. The AOD estimation was done using a combination of beamforming and a complex fitting approach (e.g., Vaudrin et al., 2018; Chau and Clahsen, 2019). Given the relatively long baselines of the
15 pentagon configuration, the altitude information was also used to remove angular ambiguities on low elevation echoes.

Based on the AODs, the detection range, the location of the transmitter and receiver sites, the Bragg vectors and incident and scattering ranges were calculated (e.g., Stober and Chau, 2015, Equation 1). AODs were obtained using Equation 2. Furthermore, the zonal and meridional winds were estimated for the same bins used for the standard Juliusruh system shown in Figure 2 after calculating Bragg vectors and the Doppler shifts (e.g., Chau et al., 2017, Equation 1).

20 The resulting parameters of the MISO-CW system are shown in Figure 4 in a similar manner to Figure 2. The salient features of these results are: (a) the wind, time, and altitude histograms are in excellent qualitative agreement with the corresponding Juliusruh results (i.e., Figure 2), (b) the number of detected meteors is about 27,000 total with about 15,500 selected with zenith angles less than 60° , (c) the 2D latitude vs longitude histograms show the expected elliptical distribution having its foci at the receiver and transmitter sites, indicated with small white circles. The 2D altitude versus inverse decay histograms are also in
25 good qualitative agreement with the SIMO-pulsed results, and the expected, small differences can be attributed to small phase offsets and the different Bragg wavelengths excited. Note that the circle in Figure 4d denotes the area of detections with zenith angles smaller than 60° with respect to the transmitter which were used to estimate the zonal and meridional winds.

4.2 MIMO-CW Results

Now we present the results for the MIMO-CW system using five linearly polarized transmitters at Kühlungsborn and five
30 circularly-polarized receivers at Neustrelitz. After applying the same decoding process used in the MISO-CW system above for each transmit-receive pair, 25 synthetic receiving channels are obtained. Recall that for each receiving antenna the complex voltages corresponding to each transmitting antenna is obtained. Figure 5 shows the RTI obtained after incoherently integrating the signals of all 25 synthetic receiver channels for the same time used in Figure 3. Given that more independent receiver signals are used, the noise variance is reduced, allowing us to observe more specular meteor echoes (more than 45).

At this point we could have proceeded by solving the location of the meteor echoes using all 25 antennas at the same time, i.e., using equation 3. In principle, this is doable and it would require converting all the measurements to a common reference

(e.g., center of the Earth) and performing beam forming from two different observing centers. To simplify the presentation of the MIMO results, here we process subsets of the 25 synthetic receivers in MISO-like and SIMO-like configurations, i.e.,
5 interferometric solutions with respect to the transmitter and receiver, using equations 2 and 1, respectively. We are leaving the use of all 25 receiving signals simultaneously, i.e., equation 3, for a future effort.

Figure 6 shows the results of the MIMO-CW system but processed in a MISO configuration (MIMO-CW MISO-like), using the information of the five transmitters in only one physical receiving antenna to obtain the AODs, Doppler shift, total range, and diffusion time. The results are in excellent qualitative agreement with the results of MISO-CW, as expected since they
10 used practically the same information. The main difference is the increased number of detections ($\sim 30,000/17,700$ instead of $\sim 27,300/15,700$ for the total/selected counts). This increased number is expected due to the increased number of synthetic receivers used for detection (25), which in turn reduces the noise variance.

The results of MIMO-CW processed in a SIMO configuration (MIMO-CW SIMO-like), using the information of only one transmitter in all five physical receiving antennas, are shown in Figure 7. Qualitatively, these results also compare very well
15 to the Juliusruh results (Figure 2). However, given that only one transmitter is used, the number of counts is slightly less than MIMO-CW MISO-like: $\sim 27,000/14,700$ instead of $\sim 30,000/17,700$ for the total/selected counts. Other salient differences with respect to MIMO-CW MISO-like are: (a) the observed specular meteor echoes close to 70 km and above 110 km, and (b) the different shape of the 2D latitude-longitude histogram. The former might be due to small remaining phase calibration issues or small imperfections in the geometry of the receiving antennas, while the latter is related to the different interferometric
20 configuration and location. For example, at Kühlungsborn there are some small hills to the South, causing different transmit and receive propagation paths particularly at very low elevation angles.

In order to have a quantitative comparison, in Figure 8 we present scatter plots of the zonal and meridional wind components using the SIMO-Pulsed (i.e., SIMO JRUH32) as a reference for: MISO-CW (first column), MIMO-CW MISO-like (second column), and MIMO-CW SIMO-like (third-column). Despite the different sampling volumes, the winds from all three configurations are highly correlated with the Juliusruh winds, presenting Pearson correlation coefficients between 0.72 and 0.82. In the
25 case of the other parameters, e.g., altitude distribution, altitude vs inverse decay time distributions, we have not done a quantitative comparison since the effective Bragg wavelengths are different between the monostatic and multistatic links. Again, by looking at panels (b) and (d) in Figures 2, 4, 6, and 7, the resulting distributions are in excellent qualitative agreement.

In Figure 9, we compare the echo location obtained with MIMO-CW MISO-like and MIMO-CW SIMO-like analyses. The
30 left panel shows the simultaneous meteor locations with both systems, color coded with altitude differences. The larger/smaller circles represent the loci of $60^\circ/30^\circ$ zenith angles with respect to each station. The center panel shows a 2D histogram (in linear scale) for latitude difference versus longitude difference. In general both approaches provide practically the same horizontal position. The observed variances in longitude and latitude are mainly due to statistical uncertainties of the AODs and AOA which are dependent on their corresponding interferometer configuration, signal-to-noise ratio and elevation angle (e.g.,
35 Holdsworth, 2005; Vaudrin et al., 2018).

The altitude difference for common detections is shown in the right panel of Figure 9 for: (1) all common detections (blue), (2) for MISO detections less than 60° zenith and SIMO detections greater than 60° zenith (yellow), and (3) for SIMO detections

less than 60° zenith and MISO detections greater than 60° zenith (green). The y-axis on the left correspond to the blue curve, while the right axis to the yellow and green results.

5 In the case of altitude, the majority of echoes present a relatively narrow distribution. The larger altitude variances are due to a mix of statistical uncertainties, small imperfections in the antenna geometries, and effective phase calibration variations at low elevations. Note that larger altitude differences in Figure 9 right panel are shown for echoes occurring further from Neustrelitz and closer to Kühlungsborn (yellow curve in Figure 9c), than from echoes closer to Neustrelitz and further from Kühlungsborn (green curve). This difference results from the Jones configuration used in Neustrelitz that has smaller baselines
10 than the pentagon configuration used in Kühlungsborn. As mentioned above, combining all 25 synthetic receivers would provide one single solution as long as the MIMO system is well phase calibrated in both transmission and reception and the antenna locations are well known with respect to a single reference, e.g., the Earth's center.

5 Discussion

A summary of the basic parameters for the different implementations presented in this work, including number of transmitters,
15 number of receivers, number of synthetic receivers per physical receiver, and counts, is shown in Table 2. Our preliminary results confirm that our novel SMR MIMO systems are suitable solutions to study the MLT atmospheric dynamics with multi-static geometries, e.g., meteor counts using one transmitter station can be increased by adding multiple single-antenna receiver stations. However, the SMR MIMO systems are not realized without their challenges.

5.1 Challenges

20 5.1.1 Implementation

As mentioned above, the implementation of our proposed systems, i.e., MIMO with coded CW diversity, are currently not possible with commercially available SMR systems, either due to hardware or software limitations. Therefore, the realization and implementation of what we propose would require major upgrades to existing systems or in-house implementation of software-defined radar procedures like those implemented in this work, accompanied with some developments in hardware
25 (e.g., VHF CW transmitters or pulsed transmitter with large duty cycles). Use of multiple sequences of pseudorandom large codes on transmission and the corresponding continuous sampling on reception are a couple of challenges with currently commercially available SMRs.

We have decided to test the MIMO concept using coded CW, which in practice is a form of spread spectrum, given the advantages described in the Introduction and in Vierinen et al. (2016). However, MIMO implementations using time diversity in pulsed systems might be possible, particularly if the separation between pulses is relative small. For example, a sequence of pulses of a few microseconds wide and a few microsecond separation between them, i.e., staggered pulses, might also work. Such a scheme can be considered as a subset of our proposed coded CW, where the code consists of -1, 0, and 1 values instead of just -1 and 1. Other groups might try to implement this or other options, if they find MIMO attractive to their studies.

5 In the case of multi-static systems, time synchronization, frequency coherence, and time stability are key to the performance of the proposed systems. In our case we have selected code sequences that are repeated every 10 milliseconds, and by using the 1 pulse-per-second from GPS receiver units, time synchronization between systems is possible within a few tens of nanoseconds precision.

5.1.2 Computation

10 The filtering and decoding required to process many channels of CW-coded links is not a trivial operation and can be computationally demanding. However, the implementation can be done nowadays in personal computers and run much faster than the acquisition time. In the end, the problem reduces to a statistical inverse problem, and as such, depending on the application and the environment, different optimal procedures are possible. For example, one can employ a maximum likelihood estimator, zero forcing, minimum mean square error, or compressed sensing, to name a few possibilities (e.g. Vierinen et al., 2016; Klein
15 et al., 1996; Jiang et al., 2011; Strohmer and Friedlander, 2009; Gao et al., 2017). In this work we have used a compressed sensing approach, given the natural sparsity of specular meteor echoes.

5.1.3 Self-noise

In terms of SNR, from the fact that we are transmitting different codes on the same frequency bandwidth one would expect a degradation of SNR, particularly if conventional codes and decoding is used. However, the selection of nearly-orthogonal
20 pseudorandom codes combined with advanced signal processing and statistical inverse problems theory make such expected SNR degradation manageable. Increasing the code length to a maximum within signal coherence and time resolution constraints allows maximization of the SNR when analyzing links individually. In that case, it is most crucial to ensure that the codes sent by each transmitter are uncorrelated at zero lag because meteors will always appear with zero relative lag between links from the same transmission site. Given the sparse nature of SMR echoes, it is also possible to analyze all of the links collectively
25 using compressed sensing approaches and minimize the effect of cross talk even further. More details on these arguments will be presented in a separate paper.

5.1.4 Cost

To facilitate the discussion on costs, we compare two multi-static systems: one using SIMO, and one using MISO. The SIMO system would consist of a single transmitter system with 25 kW peak power and 10% duty cycle and three receiving stations with five antenna interferometry capability each. The MISO system would consist of a single transmitter station with five 500-W CW transmitters with the same interferometer geometry as the receivers in SIMO and three single cross-polarized antenna located at the same places as the receivers in SIMO. In terms of transmitter costs, given that the average power is similar, the costs are expected to be similar. In the case of SIMO one pulse generator will be needed, while for MISO five pulse generators
5 are needed. On reception, the amount of hardware and space is significantly reduced for MISO, one antenna, two receiving channels, and 5 m x 5 m of area instead of five antennas, five receiving channels, and 50 m x 50 m, respectively. Taken

altogether, we expect the costs to be roughly similar, although if more links are desired, the incremental costs of MISO is much less than SIMO. A summary of these values is shown in Table 3. Note that in this simple analysis, research and development costs are not included.

10 **5.2 Advantages**

In general, we think that these challenges are worth the benefits that they enable. The field of telecommunications also faced similar challenges, but in the end the advantages of MIMO techniques (e.g., amount of information on improved channels) were much greater than the implementation costs and small losses in SNR (e.g. Telatar, 1999; Zheng and Tse, 2003). As mentioned in the Introduction, the proposed MIMO systems arose from the difficulty of building out a multi-static SMR network with
15 multiple transmitter sites and multiple interferometric receiving stations. The original idea of adding receiving antennas with interferometry capability to existing transmitter sites (Stober and Chau, 2015), although much cheaper than a single monostatic SMR station, in practice has not been easy to implement mainly due to logistical problems (area, fence, security, etc.). Our second parallel approach was to add single antenna coded CW transmitters to existing receiving arrays. The main challenge here has been dealing with societal perception of the dangers associated with a VHF transmitter near an occupied area. After a
20 couple of years of experience exploring different options to realize the benefits of spatial information and additional counts from applying multi-static SMR approaches, we have come to strongly believe that the MISO-CW and MIMO-CW configurations provide the best path forward to implement multistatic SMR networks.

5.2.1 MISO-CW

In the case of the MISO-CW, once the transmitter with interferometer capability is installed, adding more multi-static links
25 is relatively trivial. Each receiving station require only a small area, and one does not need permission to receive. The phase calibration is only necessary at one station: the transmitter site. Another scientific potential of MISO-CW is the possibility of receiving orthogonal linear (or circular) polarizations, thereby adding the ability to study polarization issues in meteor trails due to background electron density, Earth's magnetic field, and geometry. Although we are still at the testing stages, such systems could be installed in many places (e.g., in schools), and if efforts are placed to reduce the costs of hardware, deployment
30 of receiving sites could be even extended to the general public to promote citizen science. Each receiver station, aside from providing data to a given network, could integrate an engaging display of real-time MLT winds and meteor detection maps, which would be particularly attractive to the general public during meteor showers.

5.2.2 MIMO-CW

Our second proposed system, MIMO-CW, would be the equivalent of a luxury model in a commercial line of products. In terms of costs, it would be the most expensive since we would not have the benefits of simple receive stations as with MISO-CW. However, in terms of performance (number of detections, uncertainties in estimates, quality of measured parameters, separation
5 between sites, etc.) it would be the best of the two options for the same geometry. Just from the detection point of view, one

increases the number of incoherent integrations from 5 to 25, allowing the detection of weaker echoes. In terms of meteor location, AODs can be independently measured with respect to the transmitter and AOAs with respect to the receiver sites by using the information of one receiver and all the transmitters (MISO-like) and by using the information of one transmitter and all the receivers (SIMO-like), respectively, as we have done in this work. For relatively long links, detections have a larger elevation angle with respect to one of the sites than the other, therefore AOA and AOD estimates will have less uncertainty (e.g., Hocking, 2018) with a MIMO system than with either a MISO or SIMO system. As far as we know, this is the first time such simultaneous independent measurements have been done with SMRs.

Larger uncertainties in altitude are expected for low elevation angle detections (e.g., Hocking, 2018; Holdsworth, 2005; Vaudrin et al., 2018). Moreover larger uncertainties are expected for configurations with shorter antenna baselines (e.g., Holdsworth, 2005; Younger and Reid, 2017; Vaudrin et al., 2018). Therefore the altitude differences of common detections in Figure 9 are expected. Besides the statistical uncertainties, we have found that the differences are also sensitive to the precision of the interferometer geometry. These types of uncertainty are also expected in conventional SMR pulsed systems. AOA and AOD uncertainties for relatively low elevation angles could be reduced by employing larger baselines and more receiving antennas (e.g., Holdsworth, 2005), and/or by adding antennas with a significant distance in the vertical direction, e.g., an elevated antennas in the center of a pentagon (e.g., Younger and Reid, 2017). In general, having a good estimate of the AOA uncertainties can be useful in the derivation of atmospheric parameters even using low elevation meteor detections as long as such uncertainties are properly propagated and included in the inversion processes.

As mentioned above a more robust processing approach than division into MISO-like and SIMO-like configurations should provide a single meteor location, taking into account the geometry and interferometric configurations involved and the expected statistical uncertainties of AOAs and AODs. As shown by Vaudrin et al. (2018), AOA statistical uncertainties are not constant and depend on SNR, diffusion time, and zenith angle. For example, low-elevation high-SNR detections can have a small AOA uncertainty, therefore also a small altitude uncertainty, which could be smaller in that case than for detections with a high elevation angle and lower SNR. The same arguments apply to AODs. Additionally, a complete full-Earth geometry should be integrated into the full solution when combining all 25 effective channels. In terms of receiver pairs, the full solution (instead of five effective channels at a time) would increase the number of pairs from 10 to 300: 30 times more! Although a MIMO-CW implementation might not be attractive to plan from scratch in terms of logistics, it might be attractive when built on top of existing receiving systems as in our case. In future efforts, we plan to implement variants of the approach proposed by Vaudrin et al. (2018) to real data, i.e., by using a complex fitting approach, to obtain uncertainties not only on Doppler and correlation time, but also in direction cosines and therefore in location.

5.3 Comparison to monostatic

Recently Hocking (2018) has used near worst-case values of uncertainties and simple geometrical arguments to stress the potential limitations of bistatic SMR systems. Our comparison of MIMO-CW MISO-like and MIMO-CW SIMO-like corroborates some of the warnings stressed, namely the large uncertainties in AOAs experienced at low elevation angles. However, instead of seeing limitations, we would like to stress the opportunities of such systems. For example, for conservative use of

detections only at high elevation angles as is done in existing monostatic systems, multistatic systems deployed at relative short distances (between 60 and 200 km as suggested in previous works) provide a significant region of additional meteor counts with diverse observing geometries. Based on the arguments above, different interferometer configurations could be used to decrease the AOA uncertainties at low elevation angles and further increase the region of low altitude-uncertainty detections. Specifically, Holdsworth (2005) have suggested adding a fourth antenna to each Jones arm with a baseline of 20λ , and Younger and Reid (2017) have suggested adding a center antenna to a pentagon configuration with an altitude of 2.2λ . The combination of these options with our proposed MISO-CW systems would significantly increase the useful area even when conservative approaches are used. More sophisticated and aggressive approaches would require a rigorous uncertainty propagation.

An additional potential limitation to bistatic systems described by Hocking (2018) is the use of velocity estimation in certain areas, particularly the mid-point between receiver and transmitter site. As pointed out by Stober et al. (2018), a bistatic system can be interpreted as an equivalent monostatic system where: the center is the mid-point between receiver and transmitter; instead of a circle, the loci of zero radial velocity are ellipses with foci at the receiver and transmitter sites; and instead of a constant Bragg wavelength equal to $\lambda/2$, the bistatic Bragg wavelength depends on the geometry with the largest values at the mid-point. Therefore, in monostatic systems there are also regions of zero radial velocity, regions of small projected velocities (close to overhead), and of course detections at low elevation AOAs with relatively large AOA uncertainties. We agree that bistatic geometries add relative complications depending on the separation of the transmitter and receiver sites, but we want to stress that they are relative depending on the implementation, the approach used, and the application.

Finally, we also think the MIMO ideas could be applied to pulsed systems and monostatic configurations. Besides the time diversity suggested above, relatively long codes with suitable diversity (orthogonality) could be used. For example, a monostatic MIMO-pulsed configuration using code diversity has been used successfully for EEJ imaging at Jicamarca by Urco et al. (2018). This option might be attractive to existing systems. In terms of hardware, one would need to use the receiving antennas as transmitters, upgrade the number and type of transmitters to allow pseudorandom coding and a relatively long duty cycle, and reduce the number of receivers to one or two. Once the decoding is implemented, the rest of the software including detection, identification, wind analysis, etc. would still be useful. Subsequently, adding a multi-static capability would be much simpler and would allow additional counts, different viewing angles, and the spatial information of atmospheric winds.

6 Conclusions

We have introduced and tested novel SMR systems using multiple transmitters in an interferometric configuration. Such systems are shown to be good options to study the MLT region, particularly if they are used in networks with multi-static configurations. Our first system, MISO-CW, allows multistatic observations with interferometry (AODs) by having only one antenna at each receiving site. In the case of the MIMO-CW, interferometry is accomplished at both the transmitter (AODs) and receiver sites (AOAs).

In both cases the main atmospheric parameters, including the zonal and meridional winds, are in very good qualitative and
5 quantitative agreement with measurements conducted with a standard monostatic SMR located in Juliusruh. Small differences
can be attributed to the slightly different observing volumes and the different Bragg wavelengths scattered.

We have also presented for the first time two independent measurements of the same meteors, as their angular locations are
resolved from both the transmitter (MISO-like, AODs) and receiver (SIMO-like, AOAs) sites independently. We have shown
that the mean differences in horizontal distance are relatively small (a standard deviation of a few hundreds of meters). The
10 major differences are observed in altitude, although any observed large altitude differences are within the statistical uncertain-
ties of the AOAs and AODs and are known and shown to be larger at low elevation angles. Moreover, larger uncertainties are
obtained with respect to the receiver site, where the interferometer used consists of smaller baselines than those used at the
transmitter site.

The realization of our proposed and tested implementation required modern hardware practices (e.g., coded-CW) as well
15 as advanced signal processing for decoding and detection. After detection, processes used in standard systems are applicable,
including identification, AOAs and AODs estimation, wind estimation, etc.

We expect to collaborate with academic and industrial groups that are interested on our proposed systems so that the benefits
that we envision are implemented and exploited by other groups. By doing so, we expect that studies of the MLT region, e.g.,
MLT gravity waves and turbulence at scales of few kilometers to a few hundred kilometers, can be significantly improved over
different parts of the World.

Competing interests. TEXT

5 *Acknowledgements.* This work was partially supported by the Deutsche Forschungsgemeinschaft (DFG, German Research Foundation) under
SPP 1788 (CoSIP)-CH1482/3-1 and by the WATILA Project (SAW-2015-IAP-1). The authors gratefully acknowledge the support of an
international team by the International Space Science Institute (ISSI-Bern) and discussions within the ISSI Team 410. Some hardware,
software, and analysis work at MIT Haystack Observatory was supported by NSF Major Research Infrastructure grant AGS-1626041. JLC
thinks the suggestions for improvement made by D. Holdsworth. We also thank Claudia and Fred Bauske for letting us run the first proof of
10 concept at their house, and Kiara Chau for sketching our proposed systems in Figure 1.

References

- Chau, J. L. and Clahsen, M.: Empirical phase calibration for multi-static specular meteor radars using a beam-forming approach, *Radio Science*, <https://doi.org/10.1029/2018RS006741>, 2019.
- Chau, J. L., Hysell, D. L., Kuyeng, K. M., and Galindo, F. R.: Phase calibration approaches for radar interferometry and imaging configurations: Equatorial Spread F results, *Ann. Geophys.*, 26, 2333–2343, 2008.
- Chau, J. L., Stober, G., Hall, C. M., Tsutsumi, M., Laskar, F. I., and Hoffmann, P.: Polar mesospheric horizontal divergence and relative vorticity measurements using multiple specular meteor radars, *Radio Science*, 52, 811–828, <https://doi.org/10.1002/2016RS006225>, <http://dx.doi.org/10.1002/2016RS006225>, 2016RS006225, 2017.
- Elford, W.: Radar observations of meteor trails, and their interpretation using Fresnel holography: a new tool in meteor science, *Atmos. Chem. Phys.*, 4, 911 – 921, 2004.
- Foschini, G. J. and Gans, M. J.: On limits of wireless communications in a fading environment when using multiple antennas, *Wireless Personal Communications*, 6, 311–335, 1998.
- Frazer, G. J., Johnson, B. A., and Abramovich, Y. I.: Orthogonal waveform support in MIMO HF OTH radars, in: 2007 International Waveform Diversity and Design Conference, pp. 423–427, <https://doi.org/10.1109/WDDC.2007.4339454>, 2007.
- Gao, Z., Dai, L., Qi, C., Yuen, C., and Wang, Z.: Near-Optimal Signal Detector Based on Structured Compressive Sensing for Massive SM-MIMO, *IEEE Transactions on Vehicular Technology*, 66, 1860–1865, <https://doi.org/10.1109/TVT.2016.2557625>, 2017.
- Hocking, W. K.: A new approach to momentum flux determinations using SKiYMET meteor radars, *Annales Geophysicae*, 23, 2433–2439, <https://doi.org/10.5194/angeo-23-2433-2005>, <https://www.ann-geophys.net/23/2433/2005/>, 2005.
- Hocking, W. K.: Spatial distribution of errors associated with multistatic meteor radar, *Earth, Planets and Space*, 70, 93, <https://doi.org/10.1186/s40623-018-0860-2>, <https://doi.org/10.1186/s40623-018-0860-2>, 2018.
- Hocking, W. K., Fuller, B., and Vandeppeer, B.: Real-time determination of meteor-related parameters utilizing modern digital technology, *Journal of Atmospheric and Solar-Terrestrial Physics*, 63, 155–169, 2001.
- Hoffmann, P., Becker, E., Singer, W., and Placke, M.: Seasonal variation of mesospheric waves at northern middle and high latitudes, *Journal of Atmospheric and Solar-Terrestrial Physics*, 72, 1068–1079, <https://doi.org/10.1016/j.jastp.2010.07.002>, 2010.
- Holdsworth, D. A.: Angle of arrival estimation for all-sky interferometric meteor radar systems, *Radio Science*, 40, <https://doi.org/10.1029/2005RS003245>, 2005.
- Holdsworth, D. A., Reid, I. M., and Cervera, M. A.: Buckland Park all-sky interferometric meteor radar, *Radio Sci.*, 39, doi:10.1029/2003RS003 014, 2004a.
- Holdsworth, D. A., Tsutsumi, M., Reid, I. M., Nakamura, T., and Tsuda, T.: Interferometric meteor radar phase calibration using meteor echoes, *Radio Science*, 39, <https://doi.org/10.1029/2003RS003026>, <https://agupubs.onlinelibrary.wiley.com/doi/abs/10.1029/2003RS003026>, 2004b.
- Huang, Y., Brennan, P. V., Patrick, D., Weller, I., Roberts, P., and Hughes, K.: FMCW based MIMO imaging radar for maritime navigation, *Progress In Electromagnetics Research*, 115, 327–342, 2011.
- Hysell, D. L. and Chau, J. L.: Optimal aperture synthesis radar imaging, *Radio Sci.*, 41, doi:10.1029/2005RS003 383, 2006.
- Jiang, Y., Varanasi, M. K., and Li, J.: Performance Analysis of ZF and MMSE Equalizers for MIMO Systems: An In-Depth Study of the High SNR Regime, *IEEE Transactions on Information Theory*, 57, 2008–2026, <https://doi.org/10.1109/TIT.2011.2112070>, 2011.
- Jones, J., Webster, A. W., and Hocking, W. K.: An improved interferometer design for use with meteor radars, *Radio Sci.*, 33, 55–66, 1998.

- Klein, A., Kaleh, G. K., and Baier, P. W.: Zero forcing and minimum mean-square-error equalization for multiuser detection in code-division multiple-access channels, *IEEE Transactions on Vehicular Technology*, 45, 276–287, <https://doi.org/10.1109/25.492851>, 1996.
- Lau, E. M., Avery, S. K., Avery, J. P., Janches, D., Palo, S. E., Schafer, R., and Makarov, N. A.: Statistical characterization of the meteor trail distribution at the South Pole as seen by a VHF interferometric meteor radar, *Radio Science*, 41, <https://doi.org/10.1029/2005RS003247>, <https://agupubs.onlinelibrary.wiley.com/doi/abs/10.1029/2005RS003247>, 2006.
- 15 Stober, G. and Chau, J. L.: A multistatic and multifrequency novel approach for specular meteor radars to improve wind measurements in the MLT region, *Radio Science*, 50, 431–442, <https://doi.org/10.1002/2014RS005591>, <http://dx.doi.org/10.1002/2014RS005591>, 2014RS005591, 2015.
- Stober, G., Matthias, V., Brown, P., and Chau, J. L.: Neutral density variation from specular meteor echo observations spanning one solar cycle, *Geophysical Research Letters*, 41, 6919–6925, <https://doi.org/10.1002/2014GL061273>, <https://agupubs.onlinelibrary.wiley.com/doi/abs/10.1002/2014GL061273>, 2014.
- 20 Stober, G., Chau, J. L., Vierinen, J., Jacobi, C., and Wilhelm, S.: Retrieving horizontally resolved wind fields using multi-static meteor radar observations, *Atmospheric Measurement Techniques Discussions*, 2018, 1–25, <https://doi.org/10.5194/amt-2018-93>, <https://www.atmos-meas-tech-discuss.net/amt-2018-93/>, 2018.
- 25 Strohmer, T. and Friedlander, B.: Compressed sensing for MIMO radar - algorithms and performance, in: 2009 Conference Record of the Forty-Third Asilomar Conference on Signals, Systems and Computers, pp. 464–468, <https://doi.org/10.1109/ACSSC.2009.5469862>, 2009.
- Telatar, E.: Capacity of multi-antenna Gaussian channels, *European Transactions on Telecommunications*, 10, 585–595, <https://doi.org/10.1002/ett.4460100604>, <http://dx.doi.org/10.1002/ett.4460100604>, 1999.
- Urco, J. M., Chau, J. L., Milla, M. A., Vierinen, J. P., and Weber, T.: Coherent MIMO to Improve Aperture Synthesis Radar Imaging of Field-Aligned Irregularities: First Results at Jicamarca, *IEEE Transactions on Geoscience and Remote Sensing*, PP, 1–11, <https://doi.org/10.1109/TGRS.2017.2788425>, 2018.
- 30 Urco, J. M., Chau, J. L., Weber, T., and Latteck, R.: Enhancing the spatio-temporal features of polar mesosphere summer echoes using coherent MIMO and radar imaging at MAARSY, *Atmospheric Measurement Techniques*, 12, 955–969, <https://doi.org/10.5194/amt-12-955-2019>, 2019.
- 35 Valentic, T. A., Avery, J. P., Avery, S. K., and Livingston, R. C.: Self-survey calibration of meteor radar antenna arrays, *IEEE Trans. Geosci. Remote Sensing*, 35, 524–531, 1997.
- Vaudrin, C. V., Palo, S. E., and Chau, J. L.: Complex Plane Specular Meteor Radar Interferometry, *Radio Science*, 53, 112–128, <https://doi.org/10.1002/2017RS006317>, <https://agupubs.onlinelibrary.wiley.com/doi/abs/10.1002/2017RS006317>, 2018.
- Vierinen, J., Chau, J. L., Pfeffer, N., Clahsen, M., and Stober, G.: Coded continuous wave meteor radar, *Atmospheric Measurement Techniques*, 9, 829–839, <https://doi.org/10.5194/amt-9-829-2016>, <https://www.atmos-meas-tech.net/9/829/2016/>, 2016.
- Wang, J., Kwon, S., and Shim, B.: Generalized Orthogonal Matching Pursuit, *IEEE Transactions on Signal Processing*, 60, 6202–6216, <https://doi.org/10.1109/TSP.2012.2218810>, 2012.
- 505 Younger, J. P. and Reid, I. M.: Interferometer angle-of-arrival determination using precalculated phases, *Radio Science*, 52, 1058–1066, <https://doi.org/10.1002/2017RS006284>, <https://agupubs.onlinelibrary.wiley.com/doi/abs/10.1002/2017RS006284>, 2017.
- Younger, J. P., Reid, I. M., Vincent, R. A., and Murphy, D. J.: A method for estimating the height of a mesospheric density level using meteor radar, *Geophysical Research Letters*, 42, 6106–6111, <https://doi.org/10.1002/2015GL065066>, <https://agupubs.onlinelibrary.wiley.com/doi/abs/10.1002/2015GL065066>, 2015.

510 Zheng, L. and Tse, D. N. C.: Diversity and Multiplexing: A Fundamental Tradeoff in Multiple-Antenna Channels, IEEE Transactions on Information Theory, 49, 2003.

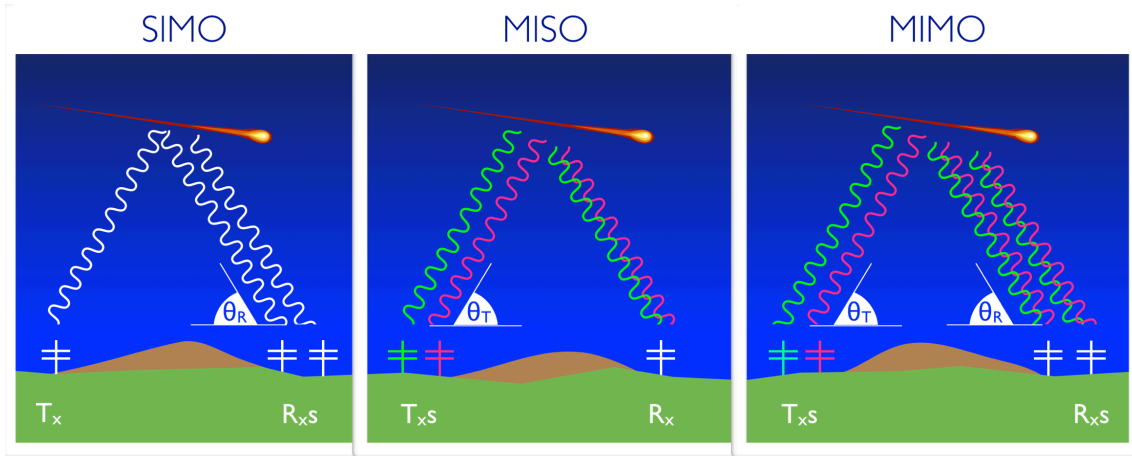


Figure 1. A sketch representing three types of SMR systems: (a) The classical system using a single transmitter and interferometry on reception ($R_{x,s}$) (SIMO), (b) a proposed system using multiple transmitter ($T_{x,s}$) in interferometer mode on transmission and a single receiver (MISO), and (c) similar to (b) but with interferometry on reception (MIMO). In the case of MISO and MIMO, the transmitter waves forms are indicated with different colors, representing different diversity (different codes in our case). Note that elevation angles are measured with respect to the transmitter (θ_T , AOD) and/or receiver (θ_R , AOA).

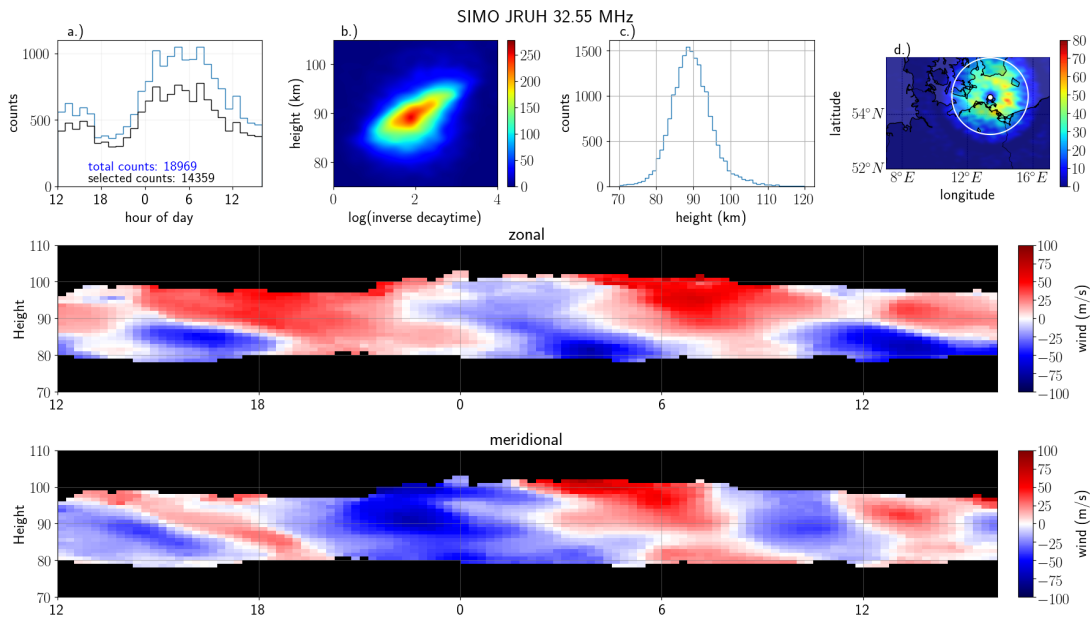


Figure 2. MLT observations with a monostatic SMR system at Juliusruh on July 11-12, 2018. The first row shows: (a) time histogram, (b) 2D histogram of altitude versus inverse decay time (log scale) color-coded in linear scale, (c) altitude histogram, (d) 2D histogram of latitude versus longitude (linear scale). The zonal and meridional winds in bins of 1 hour and 2 km are presented in the second and third rows, respectively. Note that the region of less counts in (d) is over the radar site.

2018-07-12 05:09:00

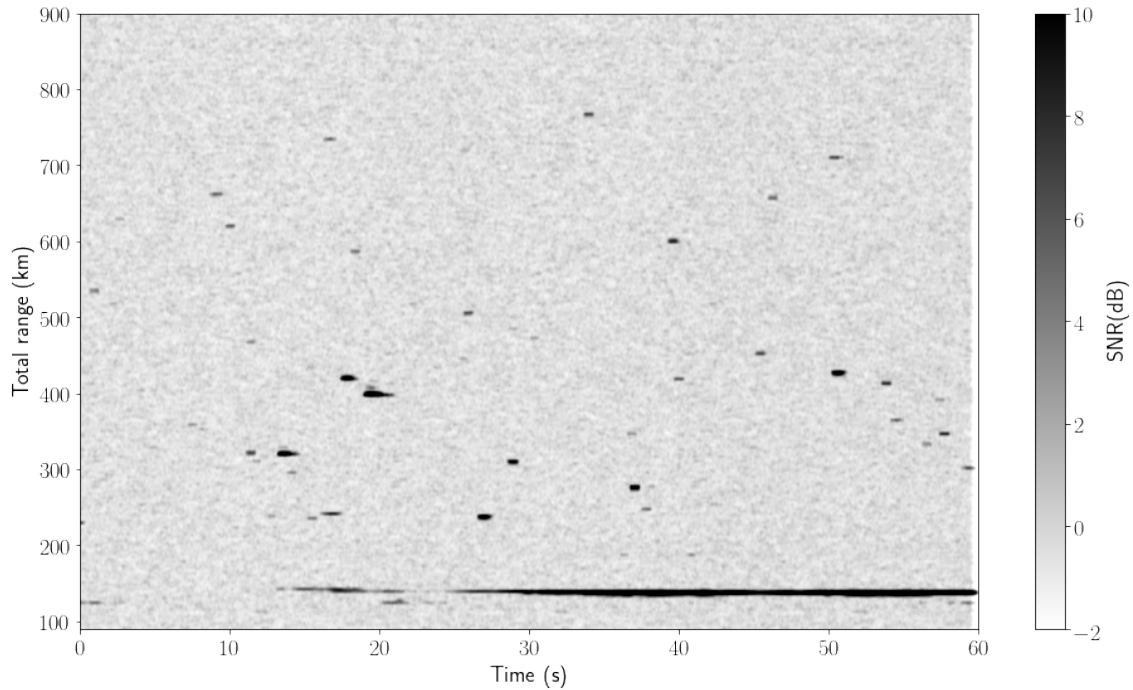


Figure 3. An example of range-time intensity plot obtained on July 12, 2018 at 0509 UT with MISO-CW. More than 30 specular meteor echoes can be observed in addition to an airplane detection. Note that total range is used, i.e., the range from the transmitter to the echo plus the range from the echo to the receiver.

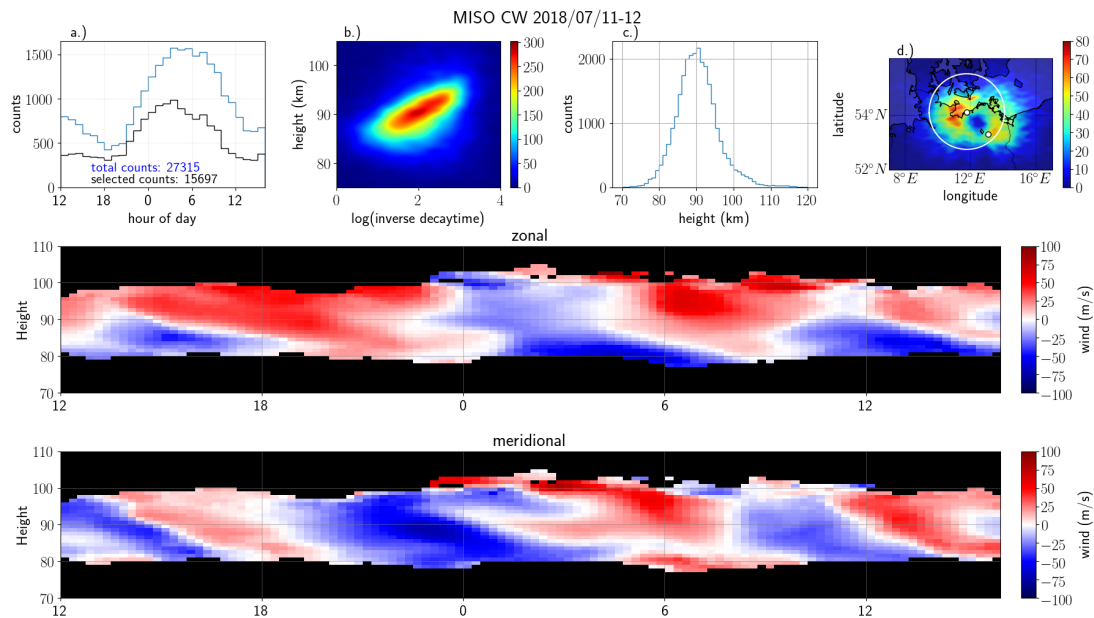


Figure 4. Similar to Figure 2 but for the MISO-CW system, i.e., the signals of 5 synthetic receivers have been incoherently integrated. The transmitter and receiver sites are indicated with small white circles in (d). Note that the region of less counts in (d) is over the mid-point of the receiver and transmitter sites.

2018-07-12 05:09:00

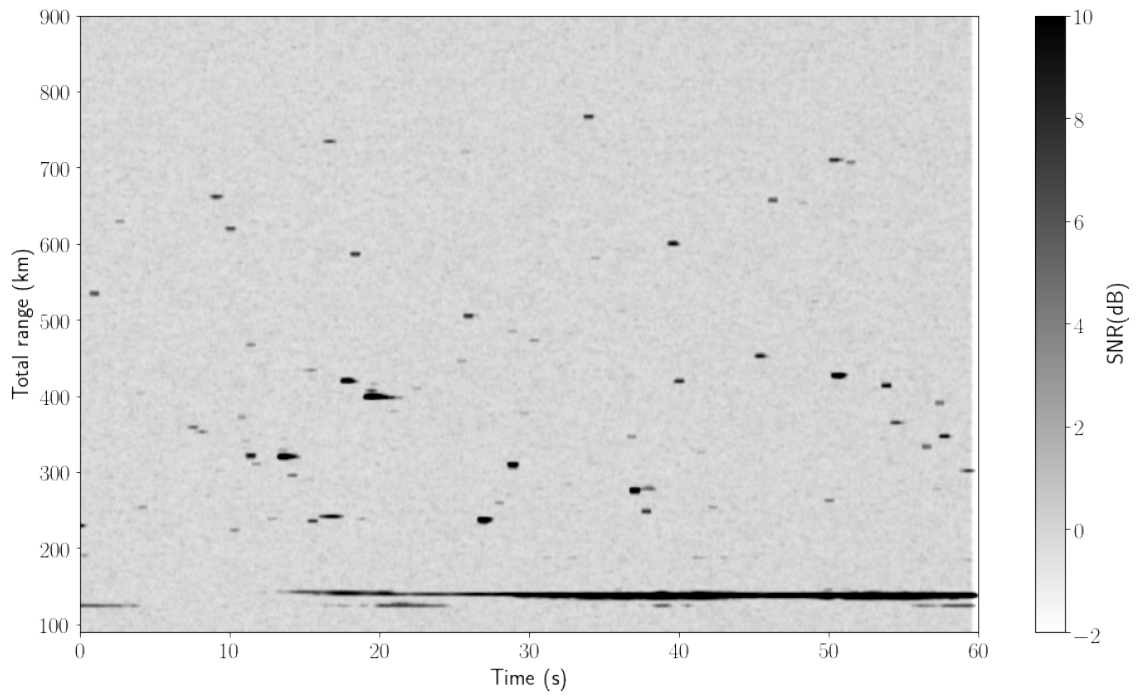


Figure 5. Similar to Figure 3 but for MIMO-CW system, i.e., the signals of 25 synthetic receiver have been incoherently integrated. More than 45 specular meteors echoes can be observed in addition to an airplane detection.

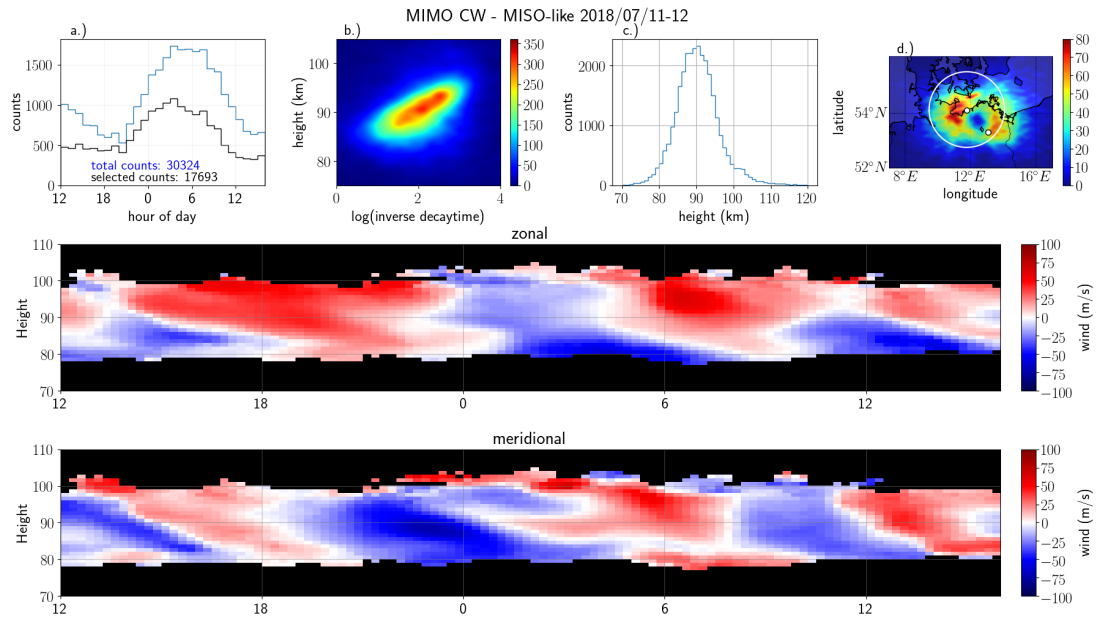


Figure 6. Similar to Figure 4 but for the MIMO-CW system applying a MISO-like analysis.

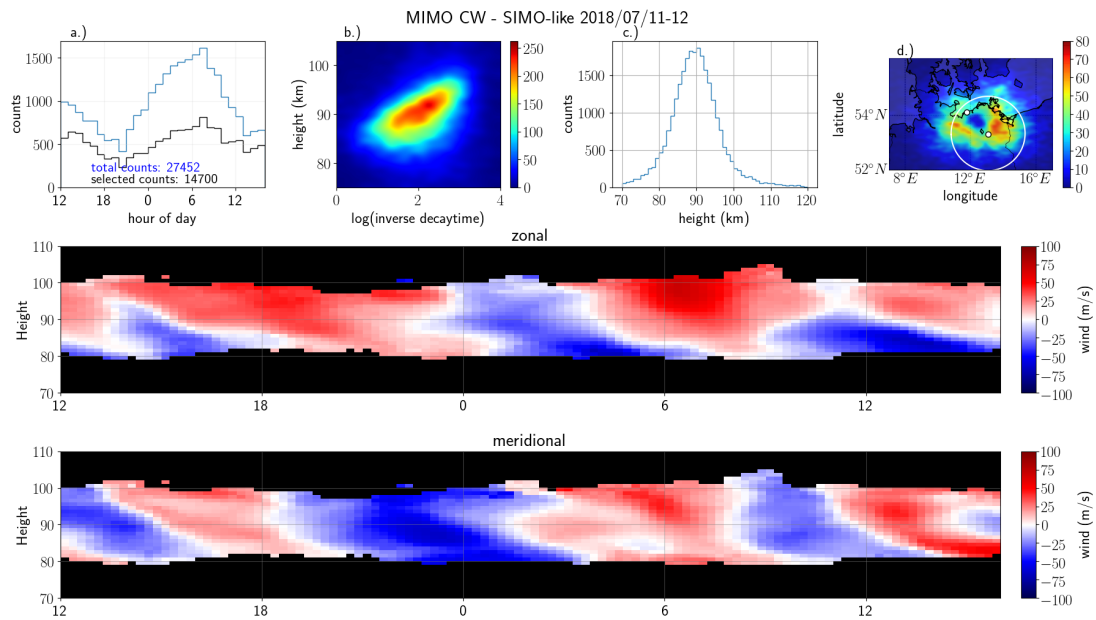


Figure 7. Similar to Figure 4 but for the MIMO-CW system applying a SIMO-like analysis.

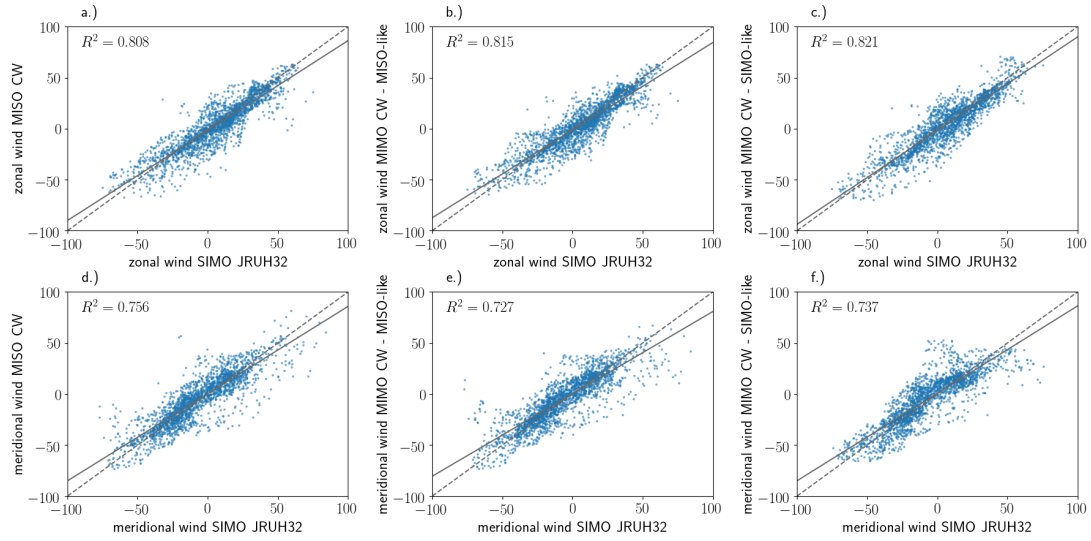


Figure 8. Scatter plots of zonal and meridional wind components using the monostatic values as a reference (SIMO-JRUH32), for: MISO-CW (first column), MIMO-CW MISO-like (second column), and MIMO-CW SIMO-like (third column). The Pearson correlation coefficients are indicated on each scatter plot.

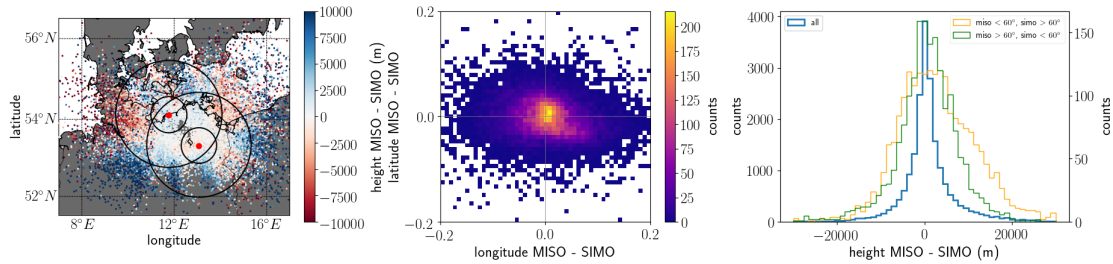


Figure 9. Comparisons of MIMO-CW MISO-like and MIMO-CW SIMO-like: (left) latitude and longitude distributions color-coded with altitude differences, (center) 2D histograms of differences in latitude and differences in longitude color coded in linear scale, and (right) histograms of altitude difference using all common detections (using left y axis). In the right panel, we also show the altitude difference histograms for MISO zenith angles less than 60° and SIMO zenith angles greater than 60° (yellow), and for MISO zenith angles greater than 60° and SIMO zenith angles less than 60° (green), using the right y axis. The loci of 30° and 60° zenith angles with respect to each site are indicated with black circles in the left panel.

Table 1. Parameters for each SMR configuration

Parameter	SIMO-Pulsed	MISO-CW	MIMO-CW
Frequency	32.55 MHz	32.0 MHz	32.0 MHz
Transmitters (Txs)	1	5	5
Tx configuration	1	Pentagon	Pentagon
Peak Power (each)	15 kW	400 W	400 W
Duty cycle	4.4 %	100 %	100 %
Inter pulse period	1.6 ms	N/A	N/A
Pulse type	coded pulsed	coded CW	coded CW
Pulse width	70 μ s	N/A	N/A
Baud width	10 μ s	10 μ s	10 μ s
Code length	7	1000	1000
Code type	Barker	Pseudo random	Pseudo random
Tx coordinates	13.3°E, 54.6 °N	11.77°E, 54.12°N	11.77°E, 54.12°N
Receivers (Rxs)	5	1	5
Rx Polarizations	1	1	1
Rx configuration	Jones	N/A	Jones
Rx sampling	10 μ s	10 μ s	10 μ s
Rx coordinates	13.3°E, 54.6 °N	13.071°E, 53.33°N	13.071°E, 53.33°N
Date of Experiments	July 11-12, 2018	July 11-12, 2018	July 11-12, 2018
Tx/Rx Separation	0	122.8 km	122.8 km

Table 2. Summary of SMR Implementations. Only detections with zenith angle respect to the reference smaller than 60° degrees are included under “Selected counts”

Technique	Number of transmitters	Number of receivers	Synthetic receivers per receiver	Interferometric solution	Total counts	Selected counts
SIMO-Pulsed	1	5	1	AOA	19,000	14,500
MISO-CW	5	1	5	AOD	27,300	15,700
MIMO-CW MISO-like	5	1	5	AOD	30,000	17,700
MIMO-CW SIMO-like	1	5	1	AOA	27,400	14,700

Table 3. Comparisons between a SIMO and a MISO multi-static system.

Parameter	SIMO Pulsed	MISO CW
Transmitter sites	1	1
Transmitters (Tx)	1	5
Tx configuration	Single	5-antenna
Polarization	Circular	Linear or Circular
Peak Power (each Tx)	25 kW	500 W
Duty cycle	10%	100 %
Pulse type	pulsed coded	coded CW
Pulse generators	1	5
Control computers	1	1
Receiving sites	3	3
Receivers (Rxs)	5	2
Rx Polarizations	1	1
Rx configuration	5-antenna	Single
Number of Rxs	5	2
Control computers	1	1
Sampling	Gated	Continuous
Receiving area	50 m \times 50 m	5 m \times 5 m